An Empirical GIS-Based Model for Landslide Potential

The empirically-based shallow landslide and debris flow model described below and used in the Nehalem Watershed Analysis is based on the most detailed field inventory of landslides and debris flows available in the Oregon Coast Range. Following the very large 1996 storm that triggered numerous landslides and debris flows in the Oregon Coast Range, the Oregon Department of Forestry (ODF) initiated a comprehensive landslide and debris flow inventory (Robison et al. 1999). To circumvent the limitations of using aerial photograph alone (i.e., many shallow slides and debris flows cannot be detected under forest canopy), a field-based inventory was conducted. Within the five study sites located in the Oregon Coast Range, landslides and debris flows were inventoried using field surveys of all channels and scour paths of landslides and debris flows. Information collected included hillside gradient, aspect, slope form, slide volume, soil characteristics, channel gradient, junction angles, etc. (see Appendix C in Robison et al. 1999 for further details on study design).

The models are designed to use field or air-photo mapped landslide locations with digital elevation models (DEM) and other GIS coverages (e.g., geology, land cover) to develop spatially distributed estimates of landslide density (refer to Miller et al. 2003, and Miller and Burnett in review). The model is intended for use over regional scales (10^2-10^4 km^2), and therefore must use readily available GIS data.

Model design and calibration uses USGS 10-m DEMs and CLAMS vegetation modeling (Coastal Landscape Analysis and Modeling Study [Ohmann and Gregory 2002]) that uses 25-m satellite imagery. Calculations are made at the resolution of the 10-m DEM, which for available USGS-provided data, reflects 40-foot contours mapped at 1:24,000 scale. Model calibration involves overlying digitized landslide inventories on basin topography and land cover, from which landslide density (e.g., number of landslides per unit area, or area of landslides per unit area) is determined as a function of topographic and land cover attributes. Other spatially distributed attributes can also be examined, geology for example, but study sites used for this calibration (Robison et al. 1999), primarily in sandstone units of the Oregon Coast Range, provided insufficient range of geologic types to resolve any influence. Topography is characterized in terms of an index function that incorporates topographic attributes thought to be important to slope stability (e.g., slope gradient, topographic convergence). An index value is calculated for each DEM pixel, from which empirical cumulative distribution functions (ECDF) are plotted for both DEM and landslide area (Figure D-1). Comparing the two ECDFs, we obtain the proportion of DEM area required to encompass a given proportion of landslide area. This curve provides criteria for evaluating different candidate index functions. Of the choices,

the index that encompasses the most landslides in the least area (i.e., isolating landslide potential) provides the best resolution of topographic controls on mapped landslide location. We evaluated three potential index functions:

1. slope gradient,
2. SHALSTAB (Montgomery and Dietrich 1994), which includes slope gradient, local topographic convergence, and total contributing area, with homogenous material properties so that variations in value are solely functions of topography, and
3. a combination of slope gradient and local topographic convergence given by $b/(A_L*S)$, where b is a measure of local topographic convergence (the length of an elevation contour crossed by flow out of the pixel, values less than one pixel length indicate convergent topography), A_L is a measure of local contributing area (within one pixel length), and S is slope gradient.

Comparison of the area versus landslide curves (Figure D-2) indicate that options three provides the best resolution of topographic controls on landslide location. This curve can be translated to a topographic weighting term, which serves as a multiplicative factor to apply to mean landslide density. The mean landslide density (total number or area of landslides divided by total area) for a particular basin, or a particular cover type, is then adjusted, pixel-by-pixel, to account for local topographic effects.

Mean landslide density was determined for four different land-cover types using CLAMS vegetation mapping (Ohmann and Gregory 2002) and an inventory of over 1,300 landslides in the Siuslaw National Forest and surrounding areas (Bush et al. 1997) associated with the February 1996 storm. Cover types were grouped into four broad categories (Miller et al. 2003):

1. *OPEN*, including non-forested areas and recent clear cuts (< 10 years),
2. *MIXED*, including hardwood stands, mixed conifer and hardwood stands, and young to intermediate-aged stands (~10-80 years),
3. *LARGE*, including old mixed hardwood and conifer and old conifer stands, and
4. *ROADS*, including all areas within 50 m of mapped roads.

The relative potential of landsliding, after accounting for topographic variability, was calculated as a percent increase above the lowest rate which was associated with the large vegetation category:

1. *OPEN:* 3.7 X lowest rate;
2. *MIXED:* 1.5 X lowest rate;

3. *LARGE:* lowest rate;
4. *ROADS:* 4.5 X lowest rate.

The effect of vegetation in the landslide model is apparent from the variation in the relative landslide rates listed above. The highest landslide density is associated with roads (i.e., 4.5 X the lowest rate which is in forests categorized as "large"). The "open" category that defines mostly recent clearcuts had the second highest rate of 3.7X. The third highest rate (i.e., 1.5 X the lowest rate which is in forests categorized as "large") is contained within "mixed" forests that are generally encompass "second growth."

In using and assessing this model, it is important to keep in mind the data on which it is built. Topographic information provided by 1:24,000 scale mapping can resolve primary features of low-order channel networks, *but may not resolve all topographic features pertinent to landslide locations* (Benda and Dunne 1997). The ability of the data to resolve topographic controls on landslide location are inherently accounted for in the calibration method, but must also be accounted for in evaluating the results. *Mapped landslide potential may not resolve smaller features, such as many topographic hollows, important to site-specific assessments*. However, mapped potential can resolve topographic controls over larger areas, such as the relative number of landslides to expect in two different first-order or larger basins.

Results of the model predictions for (1) slope gradient, (2) landslide density, (3) debris flow probability, and (4) debris flow wood recruitment corridors are found in the following Figures D-3 to D-59. The individual forest management basins covered by the slope stability and debris flow analysis include: (1) Fishhawk Management Basin (Figures D-8 – D-11), (2) Northrup Management Basin (Figures D-12 – D-15), (3) Beneke Management Basin (Figures D-16 – D-19), (4) Lousignot Management Basin (Figures D-20 – D-23), (5) Hamilton Management Basin (Figures D-24 – D-27), (6) Crawford Management Basin (Figures D-28 – D-31), (7) Sager Management Basin (Figures D-32 – D-35), (8) Buster Management Basin (Figures D-36 – D-39), (9) Quartz Management Basin (Figures D-40 – D-43), (10) Wilark Management Basin (Figures D-44 – D-47), (11) McGregor Management Basin (Figures D-48 – D-51), (12) Wheeler Management Basin (Figures D-52 – D-55), and (13) Other Contiguous Parcels (Figures D-56 – D-59).

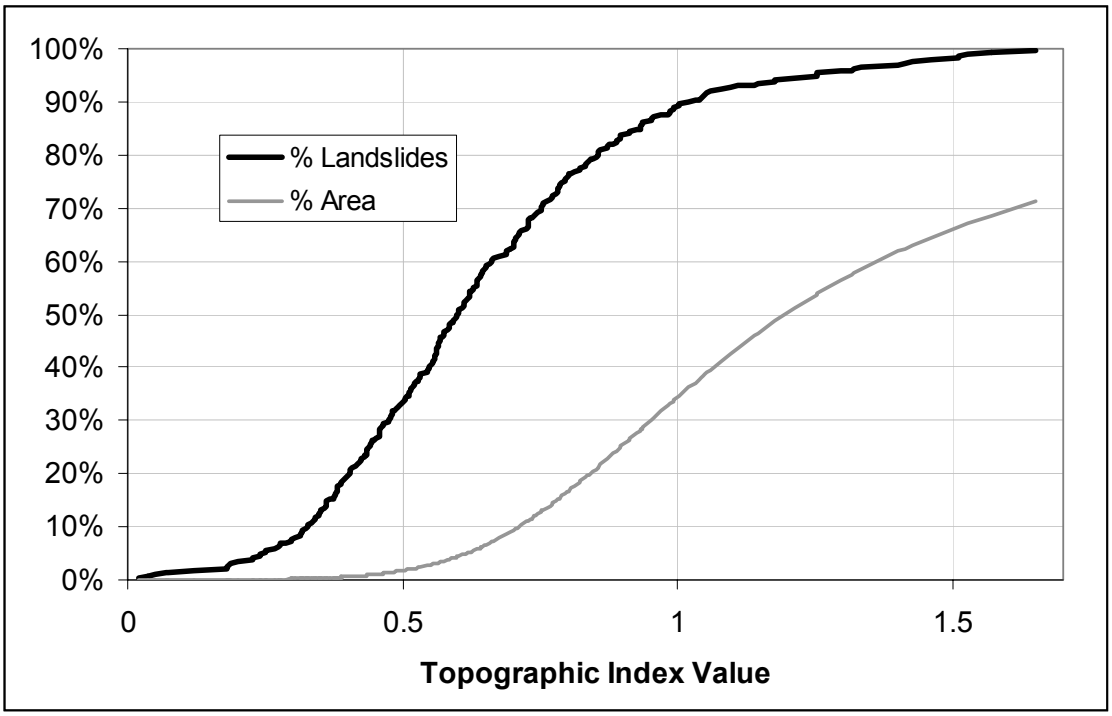

Figure D-1. Empirical cumulative distribution functions for landslides and DEM area with increasing topographic index value.

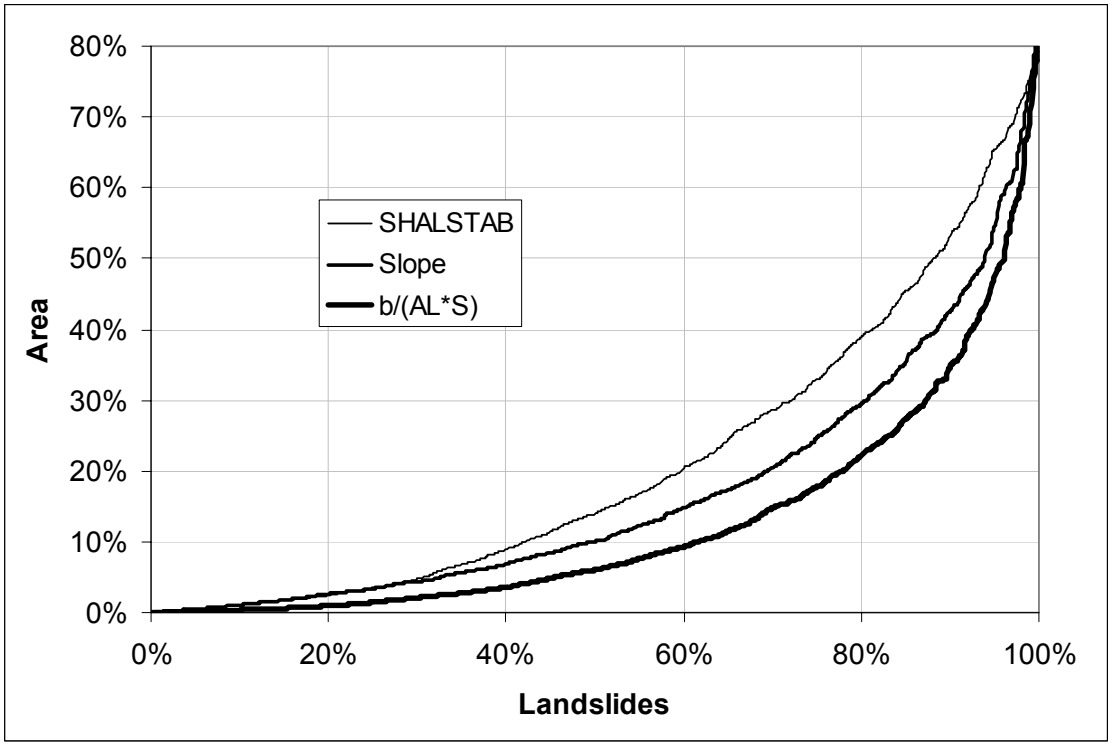

Figure D-2. Landslides vs. area curves for three potential index functions.

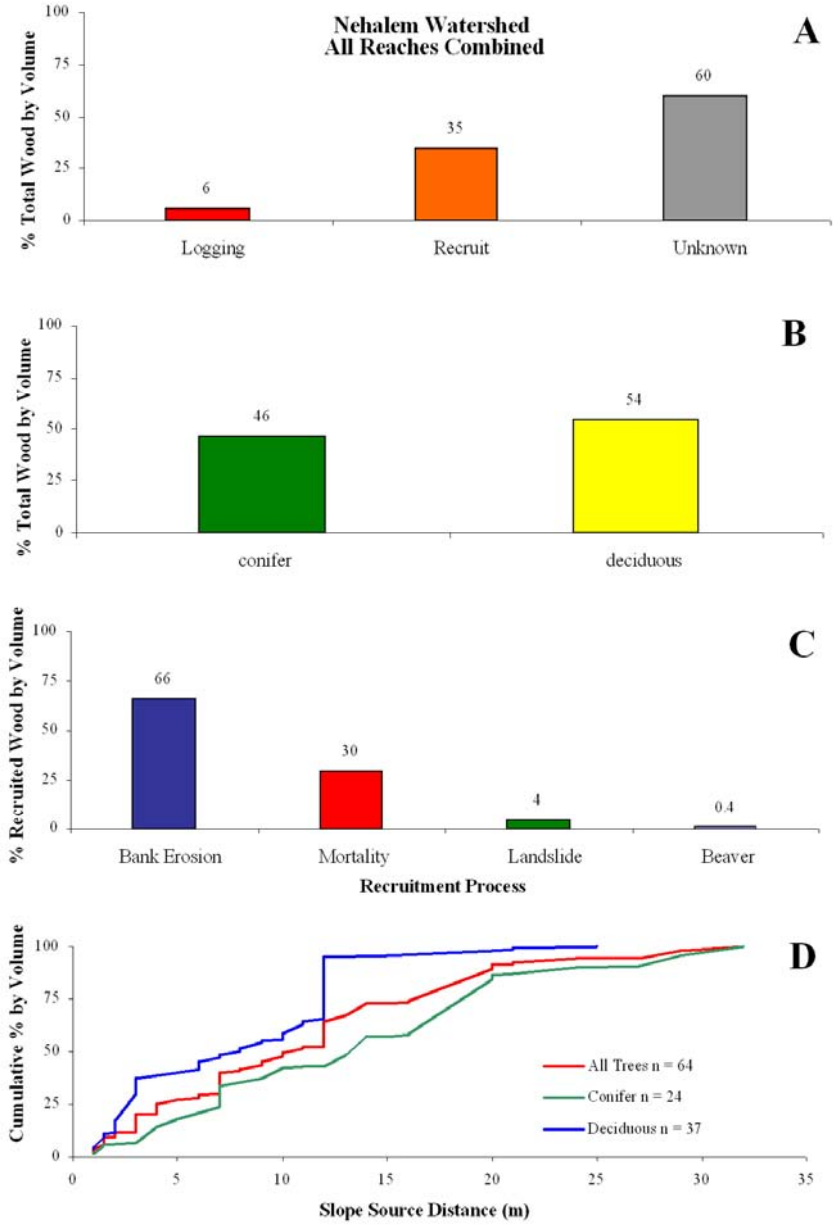

Figure D-3. Results from the preliminary wood budget analysis in the Nehalem Watershed. (A) Measured wood was categorized according to source including logging, recruited wood (i.e., identifiable to a source such as mortality, bank erosion, or landsliding), and unknown (i.e., cannot be identified to a source). (B) Measured wood was categorized as either conifer or deciduous. (C) Of the identifiable wood (approximately 35% of the total), bank erosion dominated wood recruitment (66%) followed by mortality (30%) and landslide (4%). (D) Source distance curves indicate how far from the stream that wood is entering the channel. For example, 90% of conifer wood enters the channel from approximately 90 ft away.

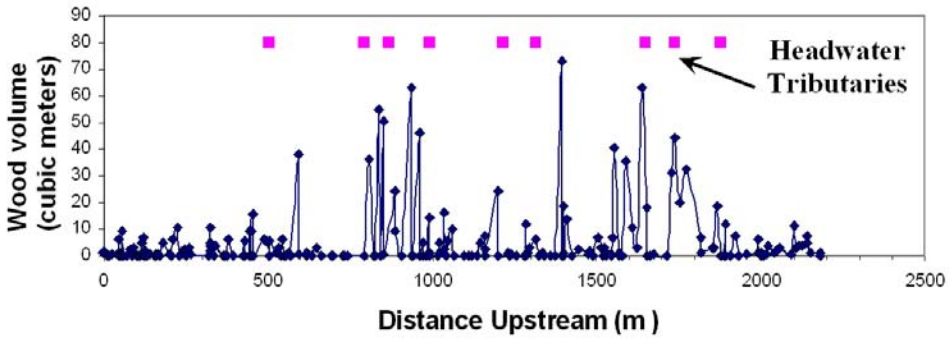

Figure D-4.Apparent spatial relationship between the highest wood loadings and debris flow-prone headwater tributaries along a fourth order tributary in the Nehalem watershed.

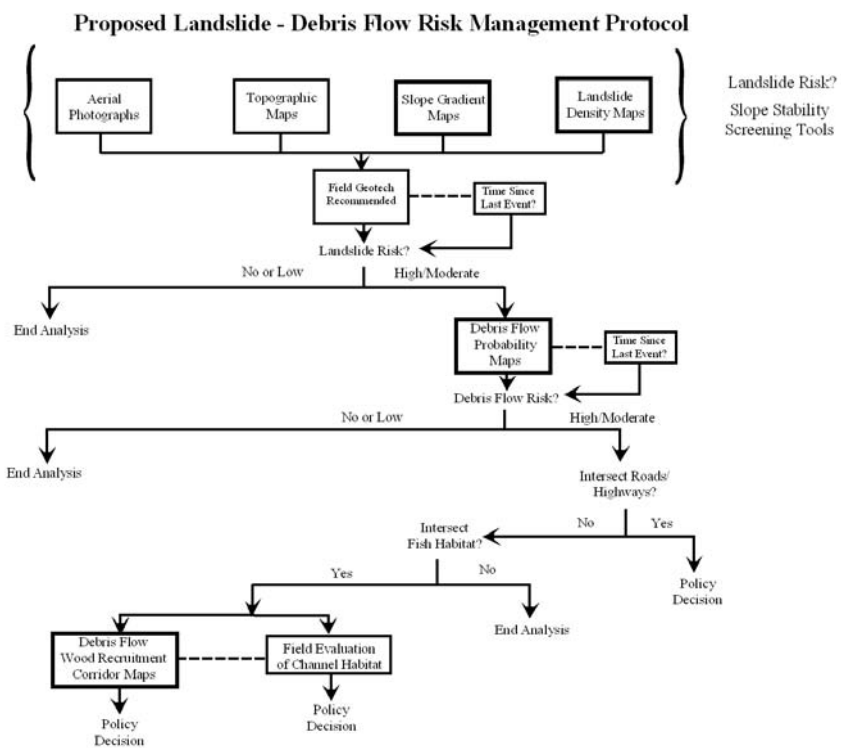

Figure D-5. A proposed shallow landslide – debris flow risk management protocol (see Benda et al. 2005 for further discussion). The heavy line boxes refer to the predictions of shallow landslide and debris flow potential made in the Nehalem watershed study area.

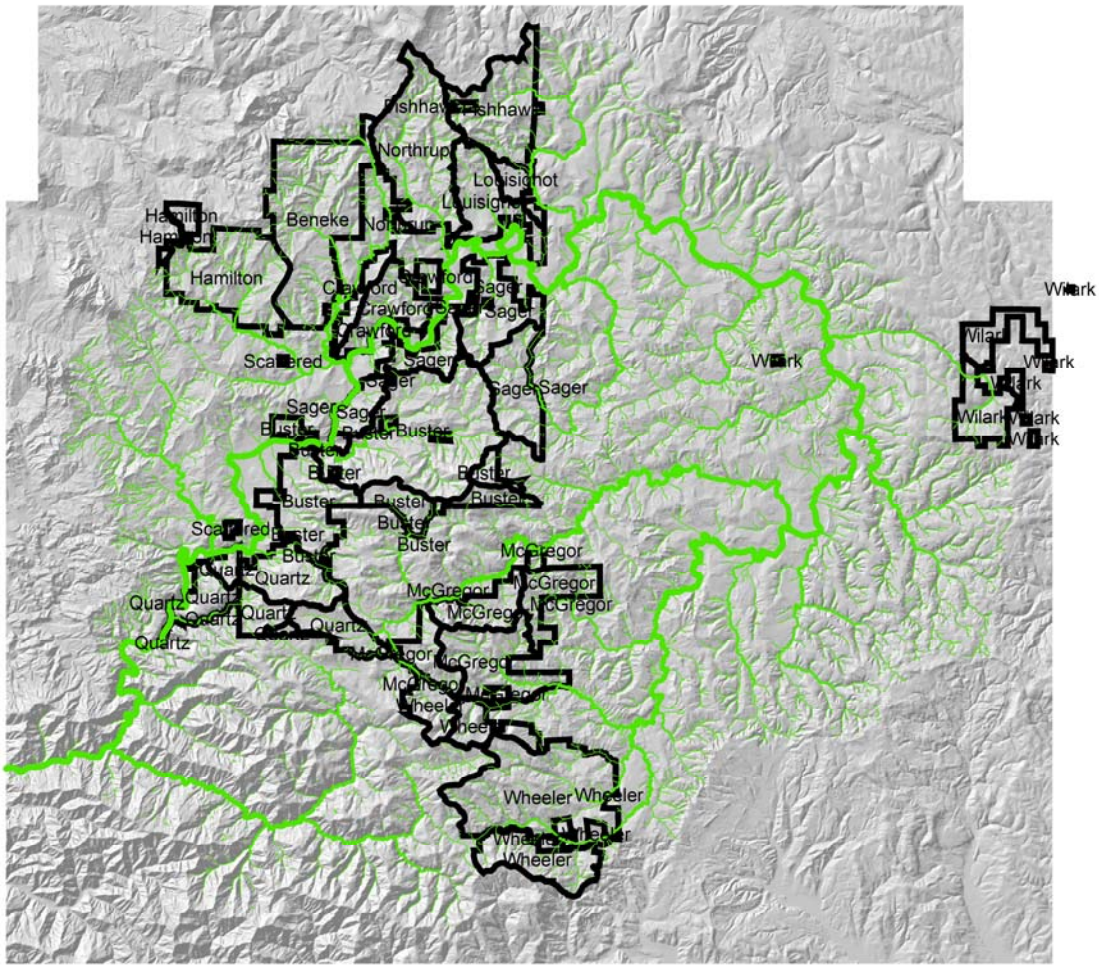

Figure D-6. The locations of the Oregon Department of Forestry Management Basins. The landslide and debris flow analysis was conducted at the HUC 6th field and each management basin overlaps with one to three 6th-field HUCs.

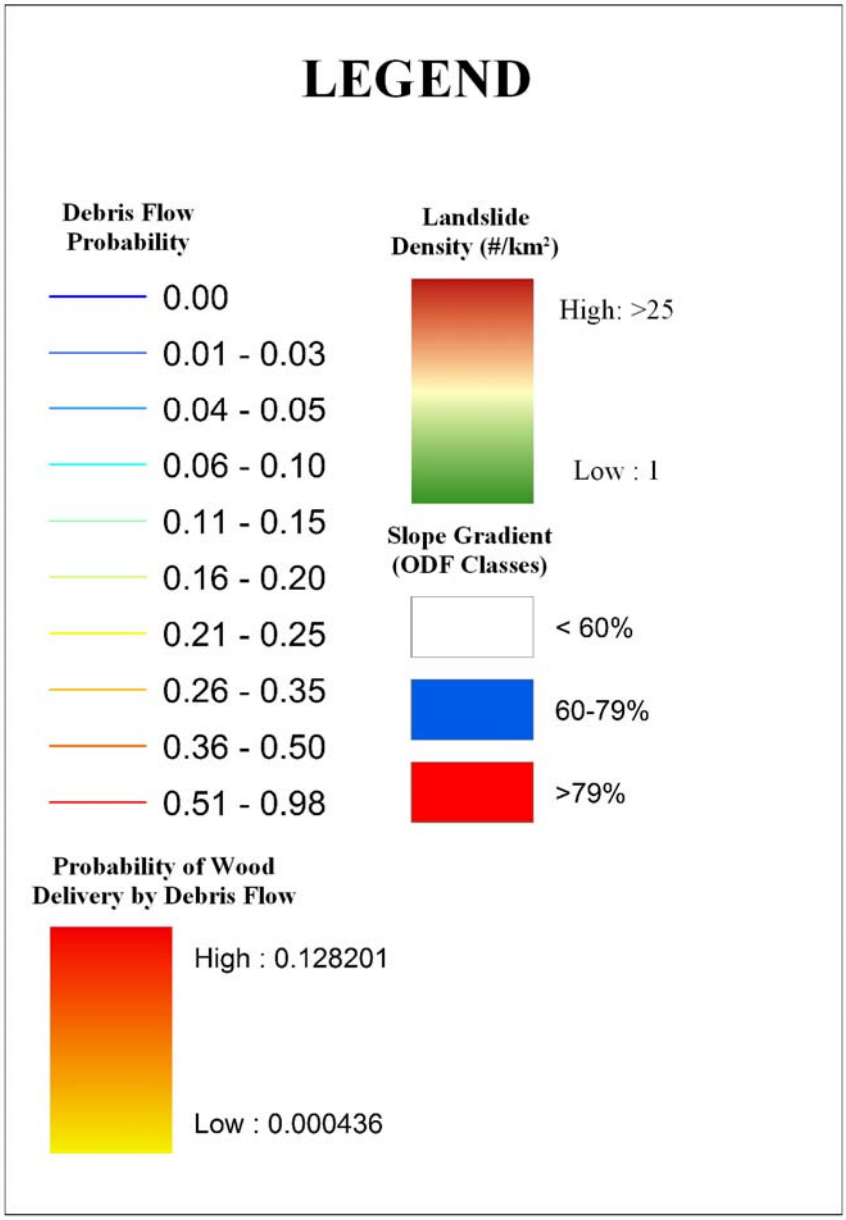

Figure D-7. Legend for the landslide and debris flow maps used in the Nehalem Watershed Analysis. Refer to Table 7-1 and discussion of models for more details.

7. FISH HAWK MANAGEMENT BASIN

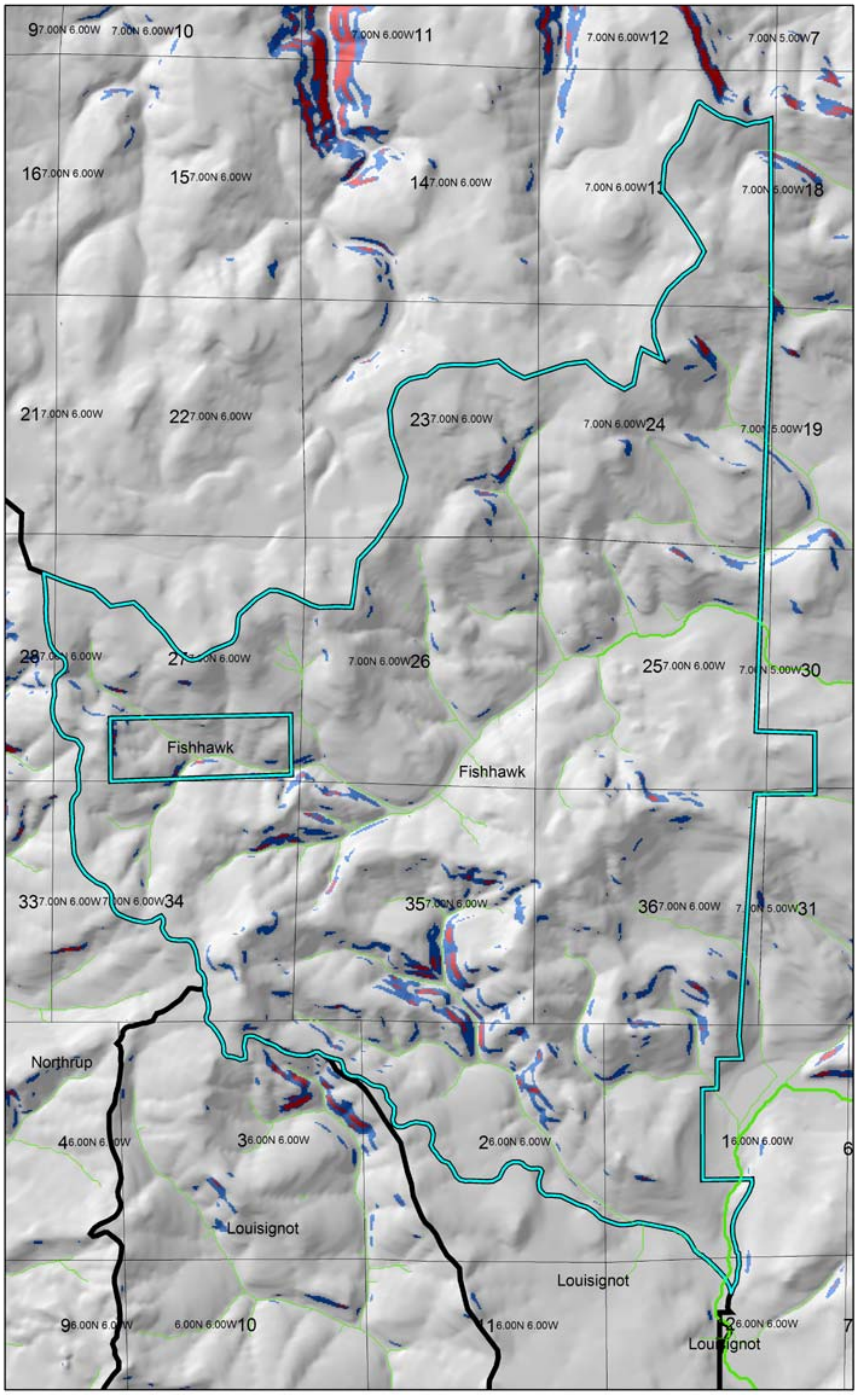

Figure D-8. Slope gradient map for the FishHawk Management Basin. Refer to the Legend in Figure D-7.

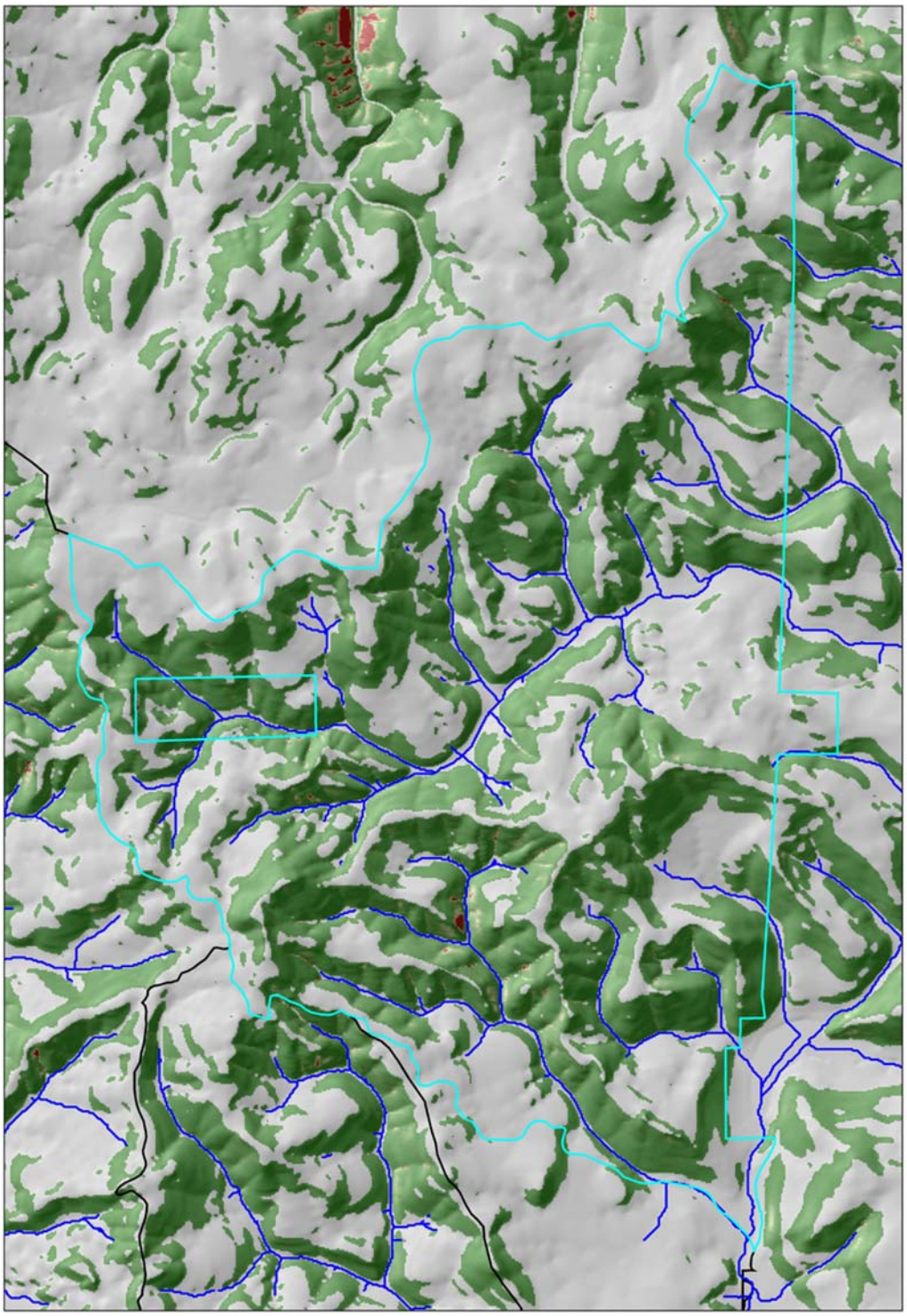

Figure D-9. The predicted landslide density for the FishHawk Management Area. Refer to the Legend in Figure D-7; the gray areas have no predicted landslide density.

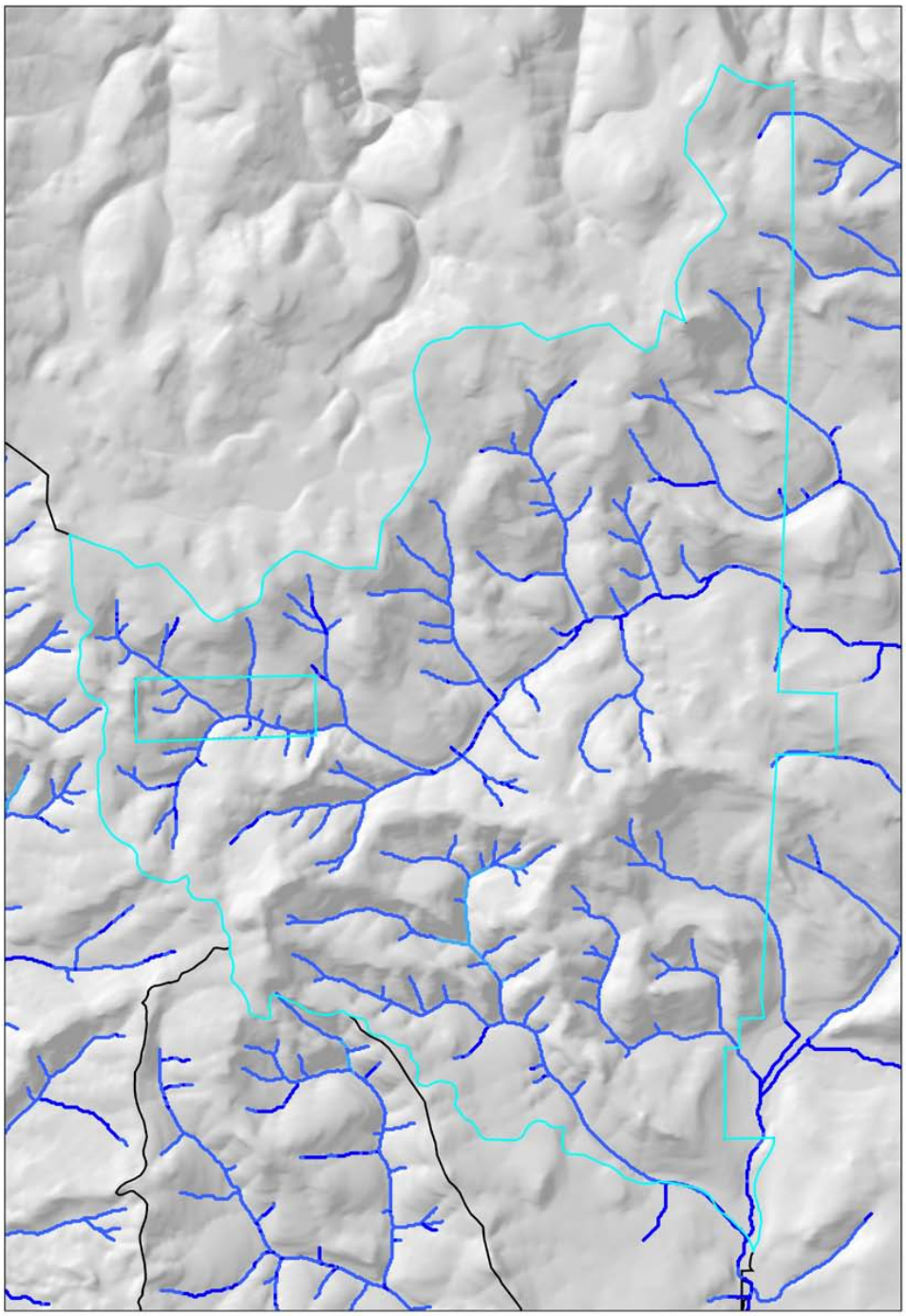

Figure D-10. The predicted debris flow probability for the FishHawk Management Area. Refer to the Legend in Figure D-7. The predicted probabilities reflect cumulative landslide densities (that could trigger debris flows) and not individual pixel-based landslide potential shown in the landslide density map.

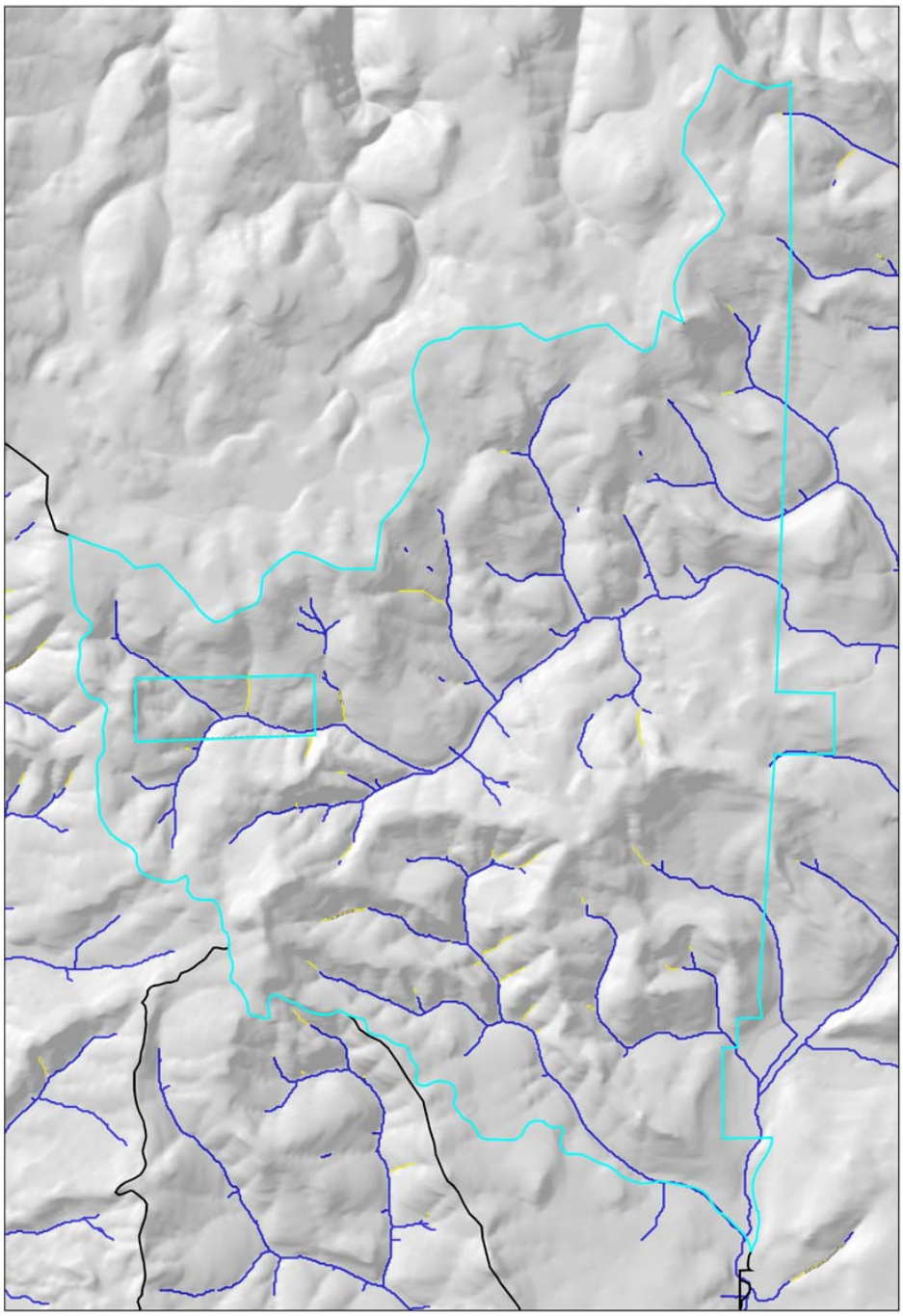

Figure D-11. Headwater streams predicted to contribute wood to larger, fish-bearing streams in the FishHawk Management Area. Refer to the Legend in Figure D-7. The predicted probabilities reflect cumulative landslide densities (that could trigger debris flows) and not individual pixel-based landslide potential shown in the landslide density map.

8. NORTHRUP MANAGEMENT BASIN

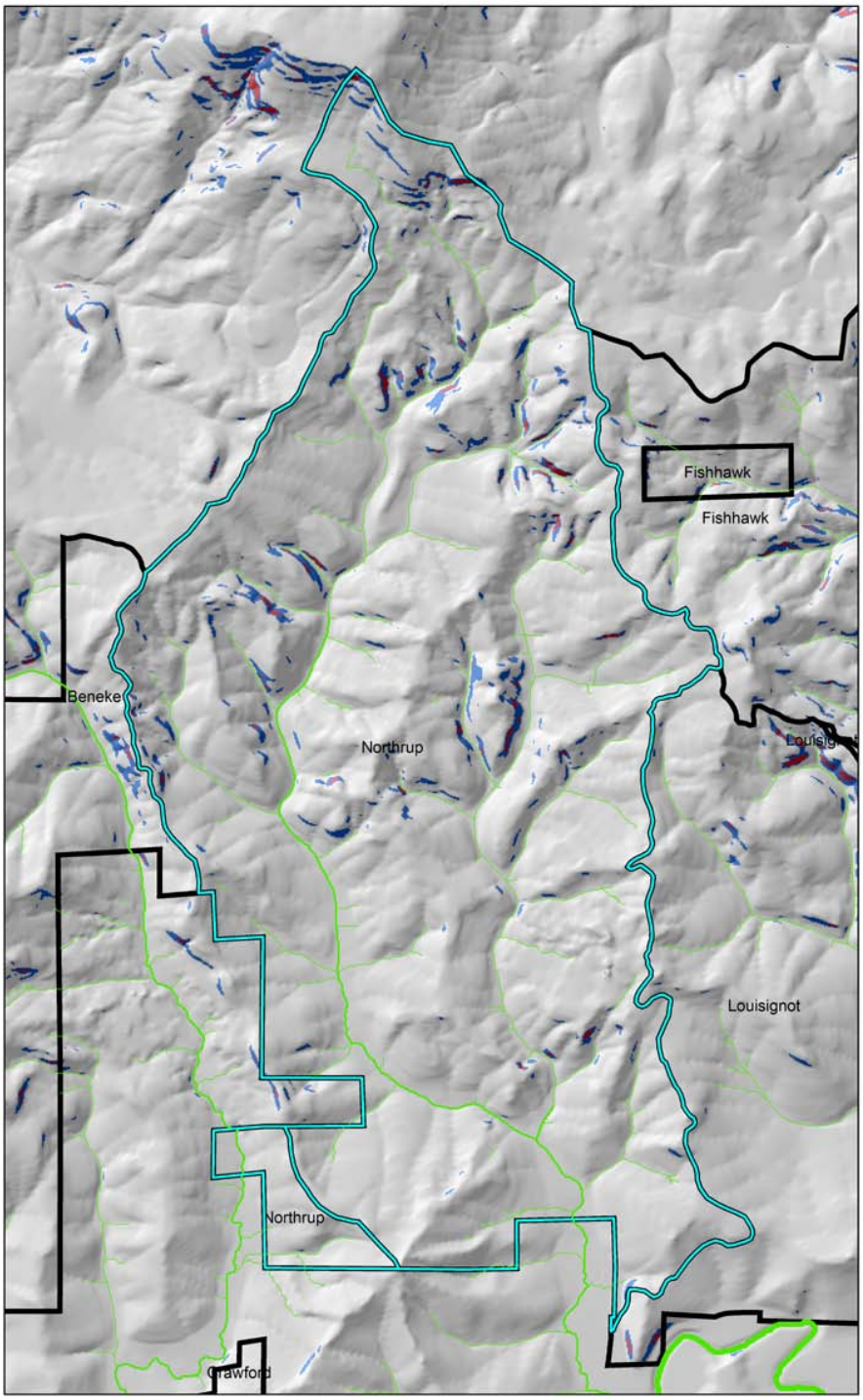

Figure D-12. Slope gradient map for the Northup Management Basin. Refer to the Legend in Figure D-7.

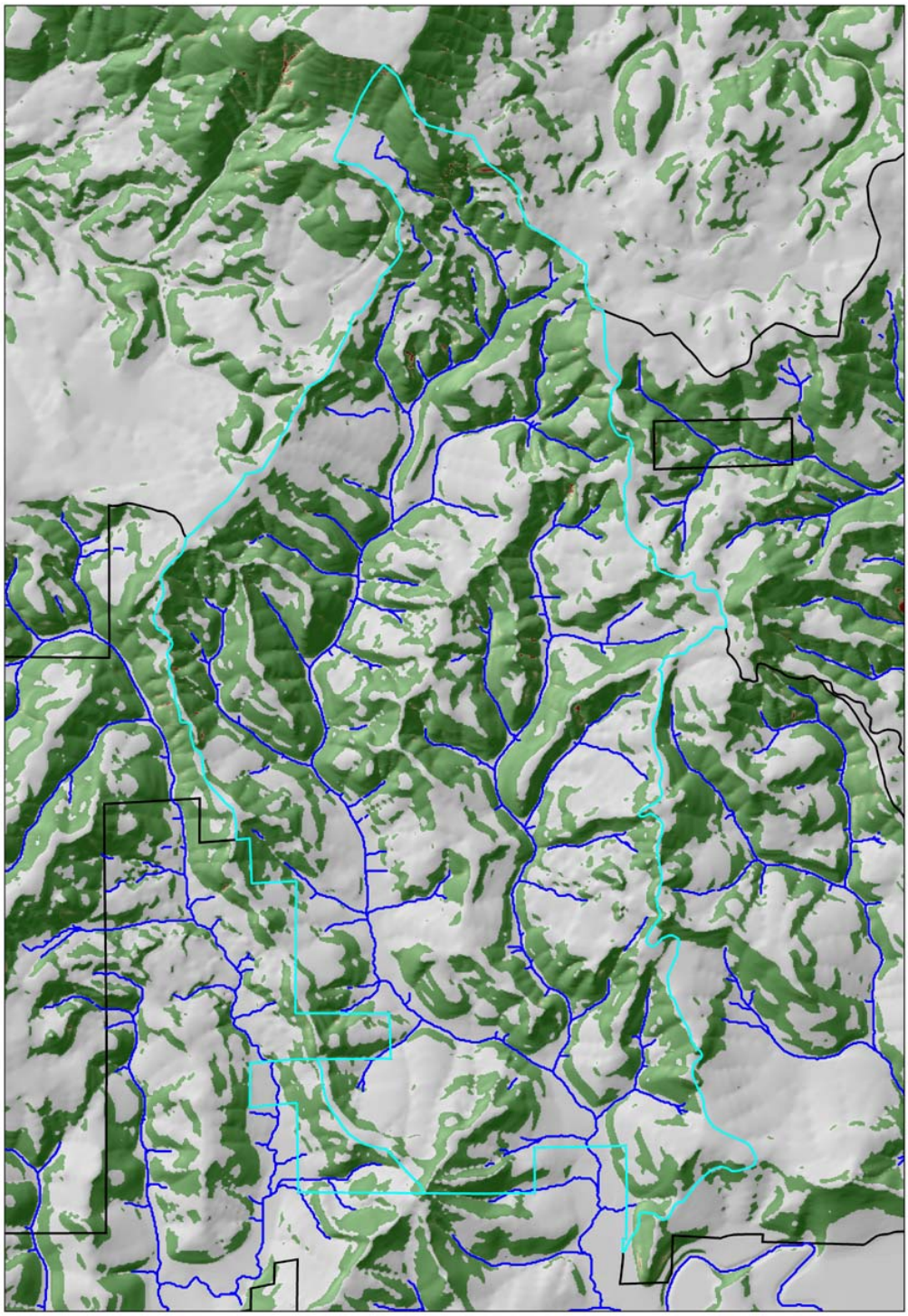

Figure D-13. Predicted landslide density for the Northup Management Basin. Refer to the Legend in Figure D-7; the gray areas have no predicted landslide density.

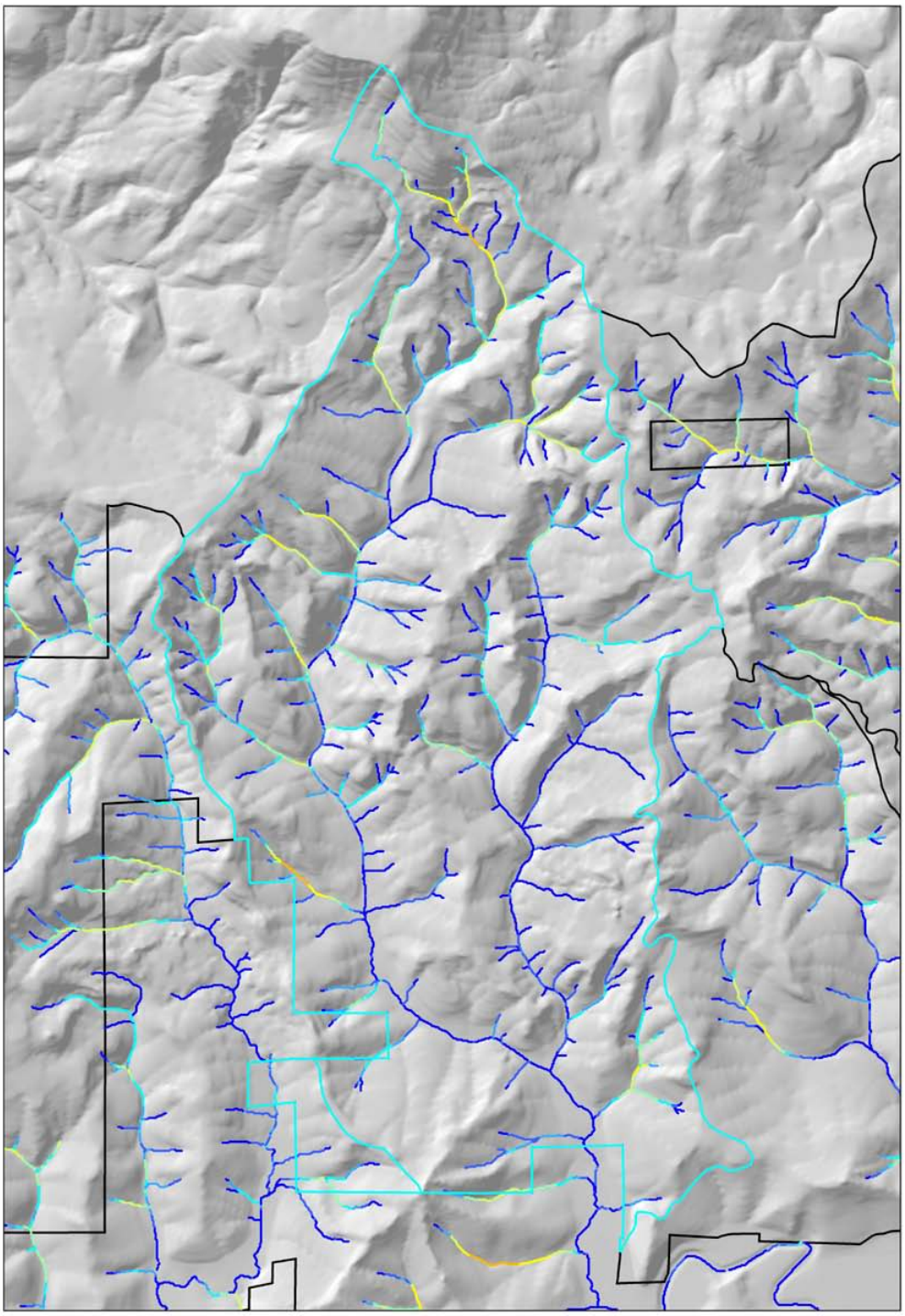

Figure D-14. Predicted debris flow probability for the Northup Management Basin. Refer to the Legend in Figure D-7. The predicted probabilities reflect cumulative landslide densities (that could trigger debris flows) and not individual pixel-based landslide potential shown in the landslide density map.

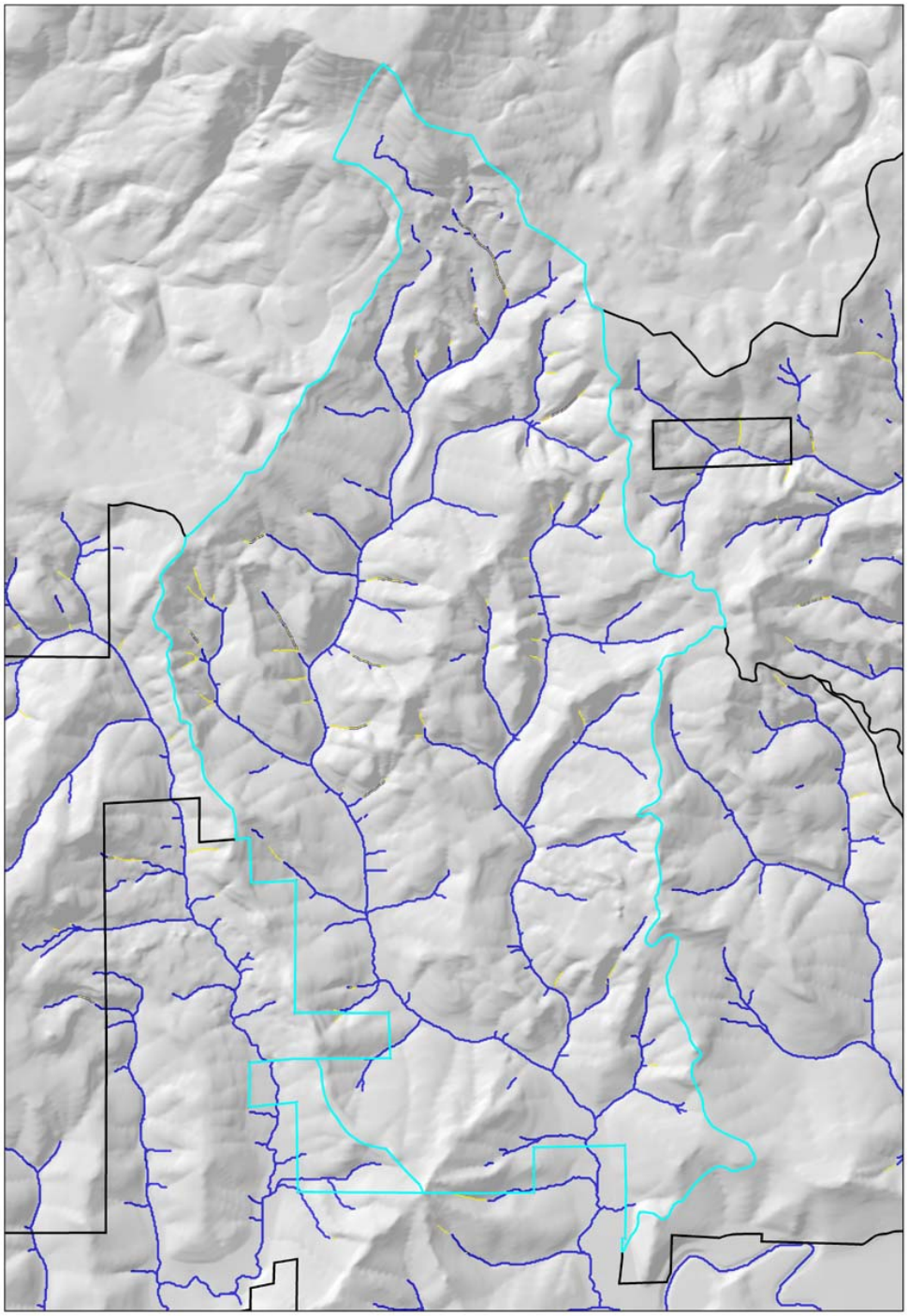

Figure D-15. Predicted headwater streams that contributed wood to fish-bearing channels by debris flows for the Northup Management Basin. Refer to the Legend in Figure D-7; predictions apply to headwater streams only. The predicted probabilities reflect cumulative landslide densities (that could trigger debris flows) and not individual pixel-based landslide potential shown in the landslide density map.

BENEKE MANAGEMENT BASIN

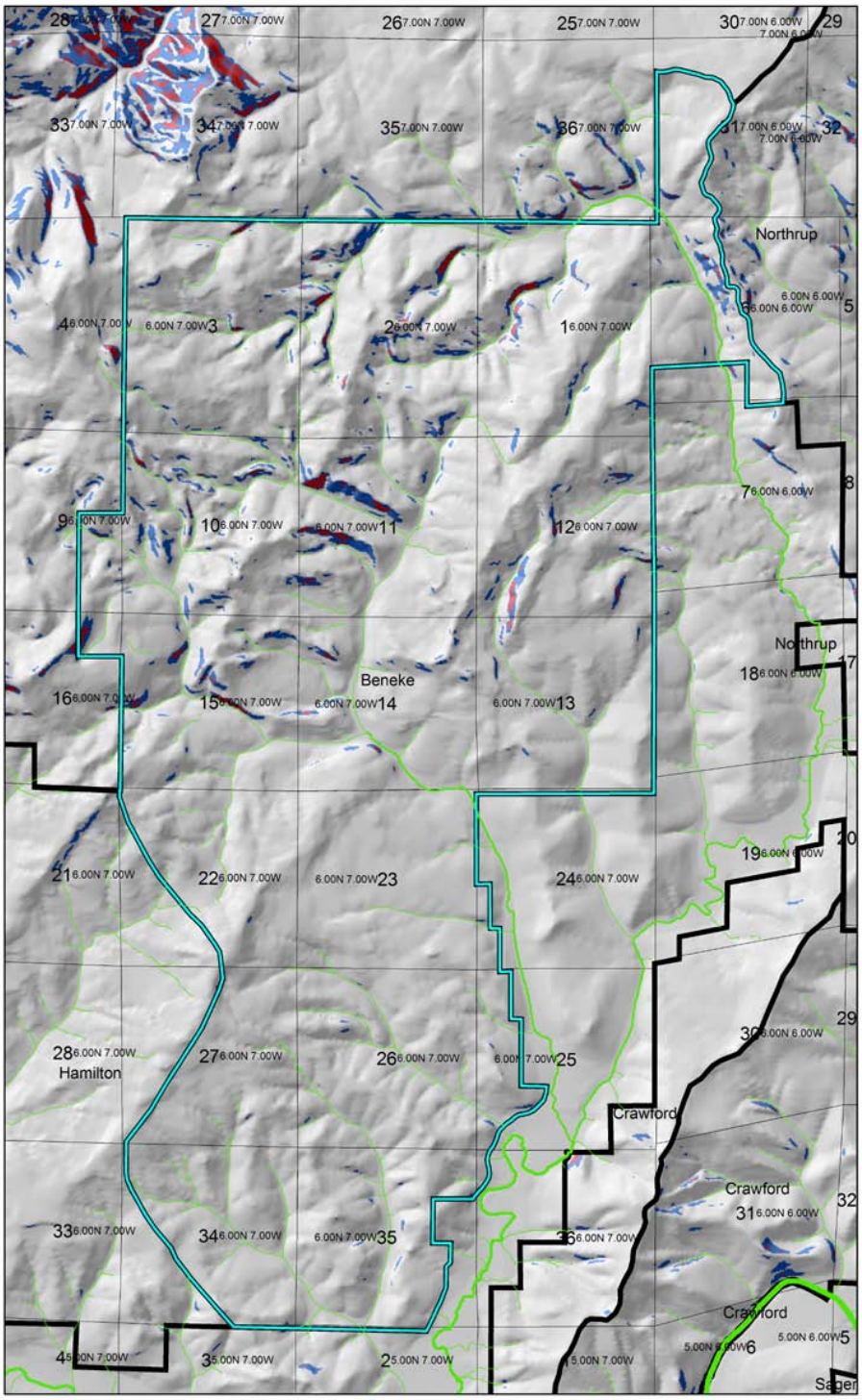

Figure D-16. Slope gradient map for the Beneke Management Basin. Refer to the Legend in Figure D-7.

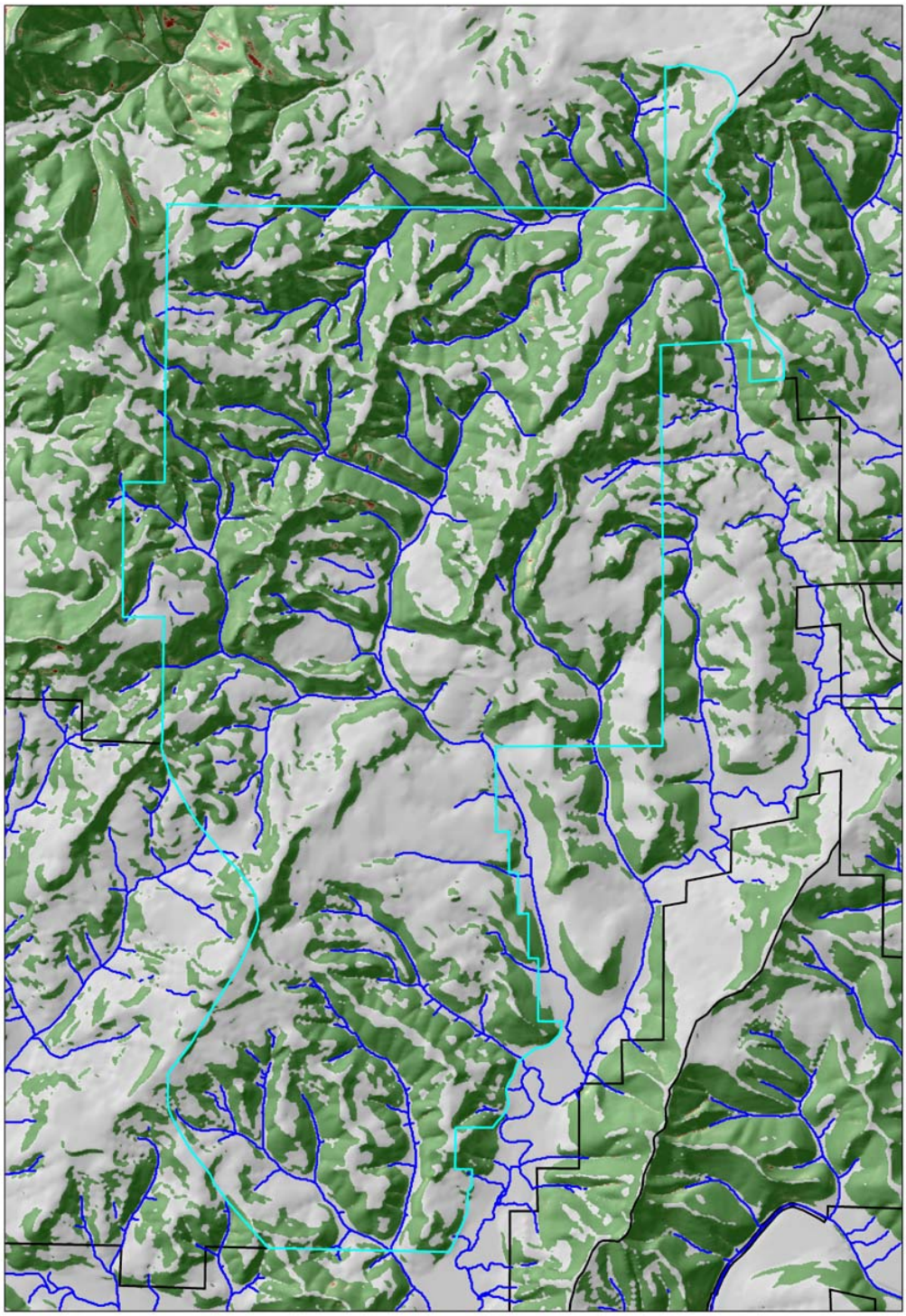

Figure D-17. Predicted landslide density for the Beneke Management Basin. Refer to the Legend in Figure D-7; the gray areas have no predicted landslide density.

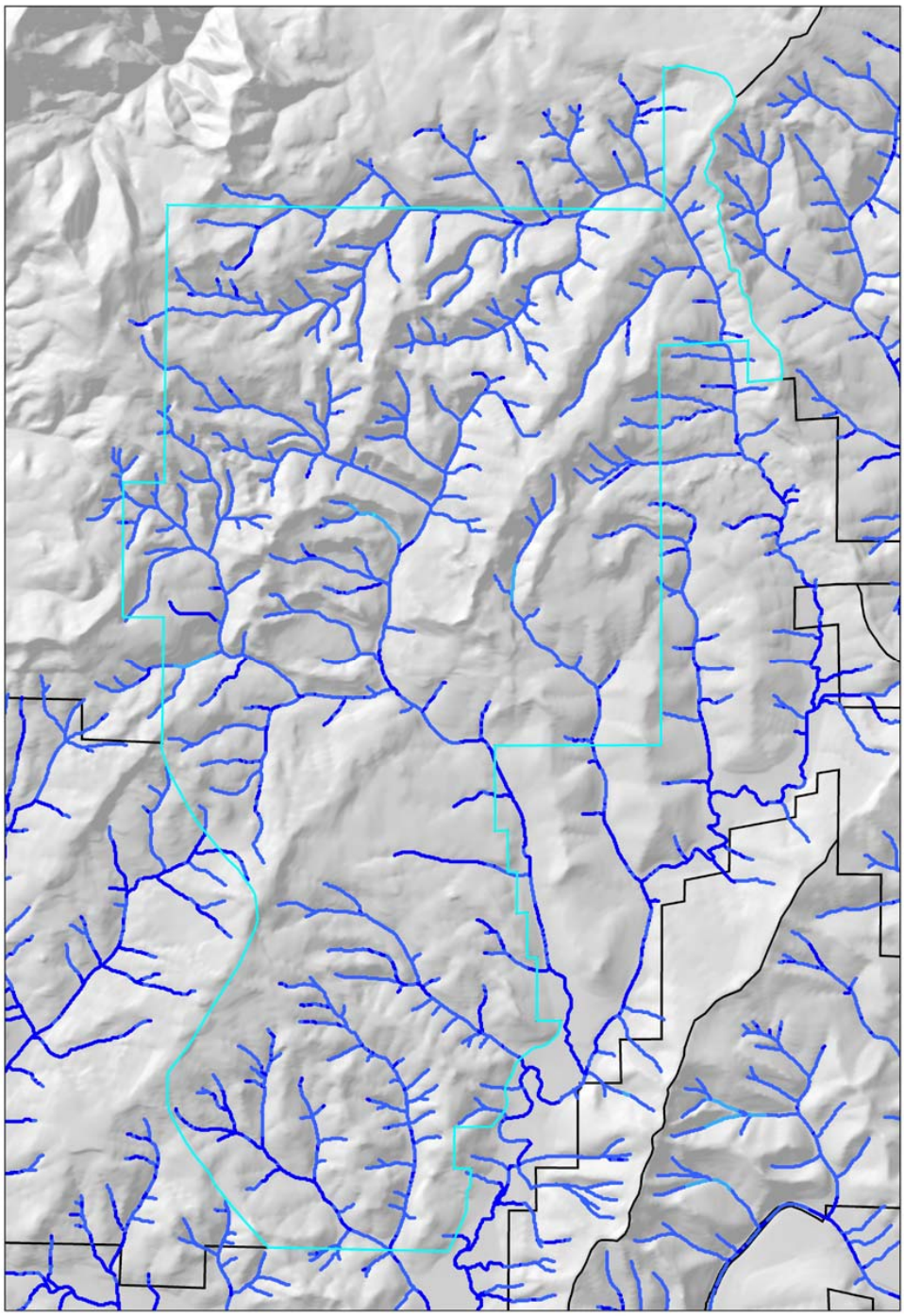

Figure D-18. Predicted debris flow probability for the Beneke Management Basin. Refer to the Legend in Figure D-7. The predicted probabilities reflect cumulative landslide densities (that could trigger debris flows) and not individual pixel-based landslide potential shown in the landslide density map.

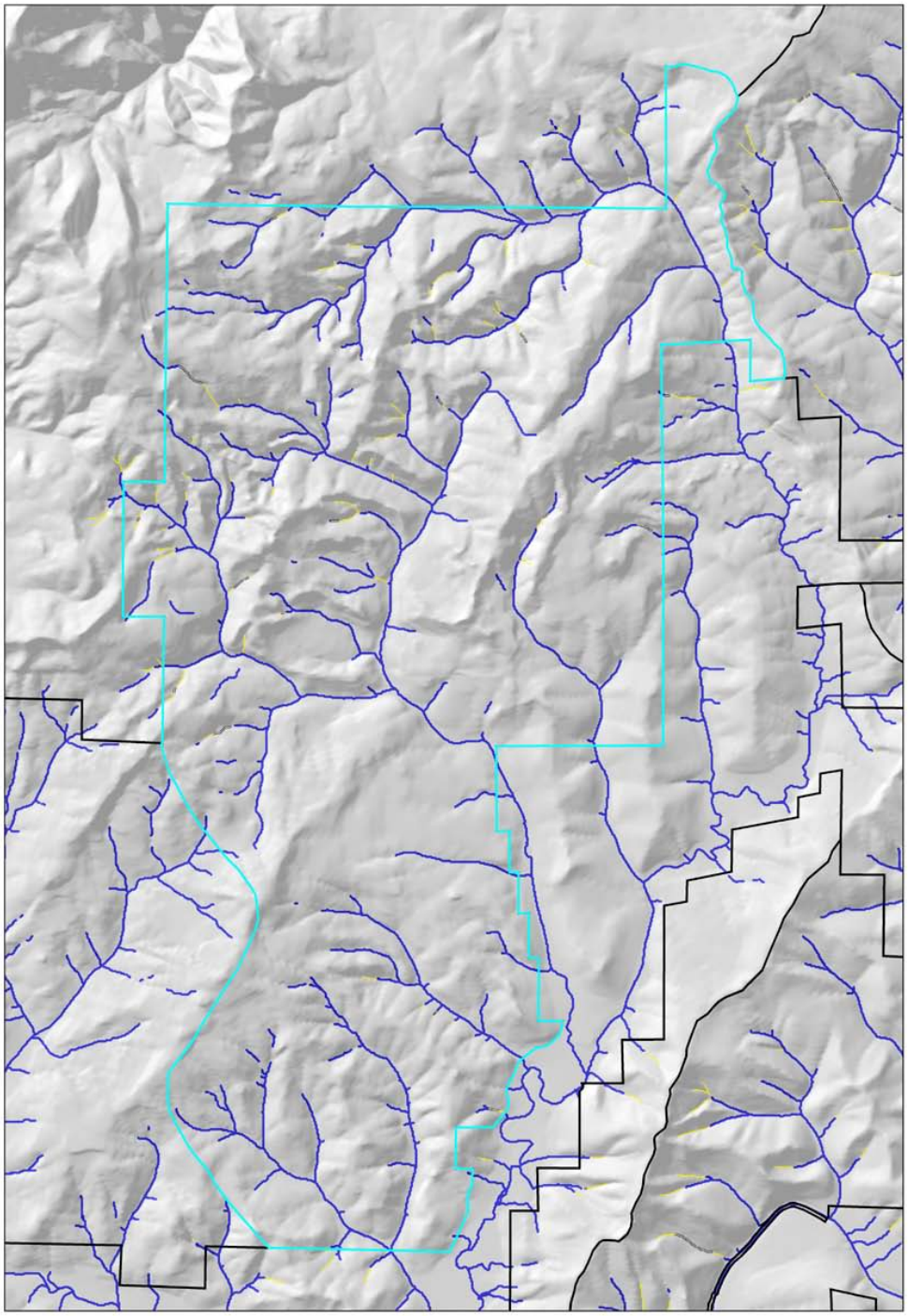

Figure D-19. Predicted headwater streams that contributed wood to fish-bearing channels by debris flows for the Beneke Management Basin. Refer to the Legend in Figure D-7; predictions apply to headwater streams only. The predicted probabilities reflect cumulative landslide densities (that could trigger debris flows) and not individual pixel-based landslide potential shown in the landslide density map.

9. LOUISIGNOT MANAGEMENT BASIN

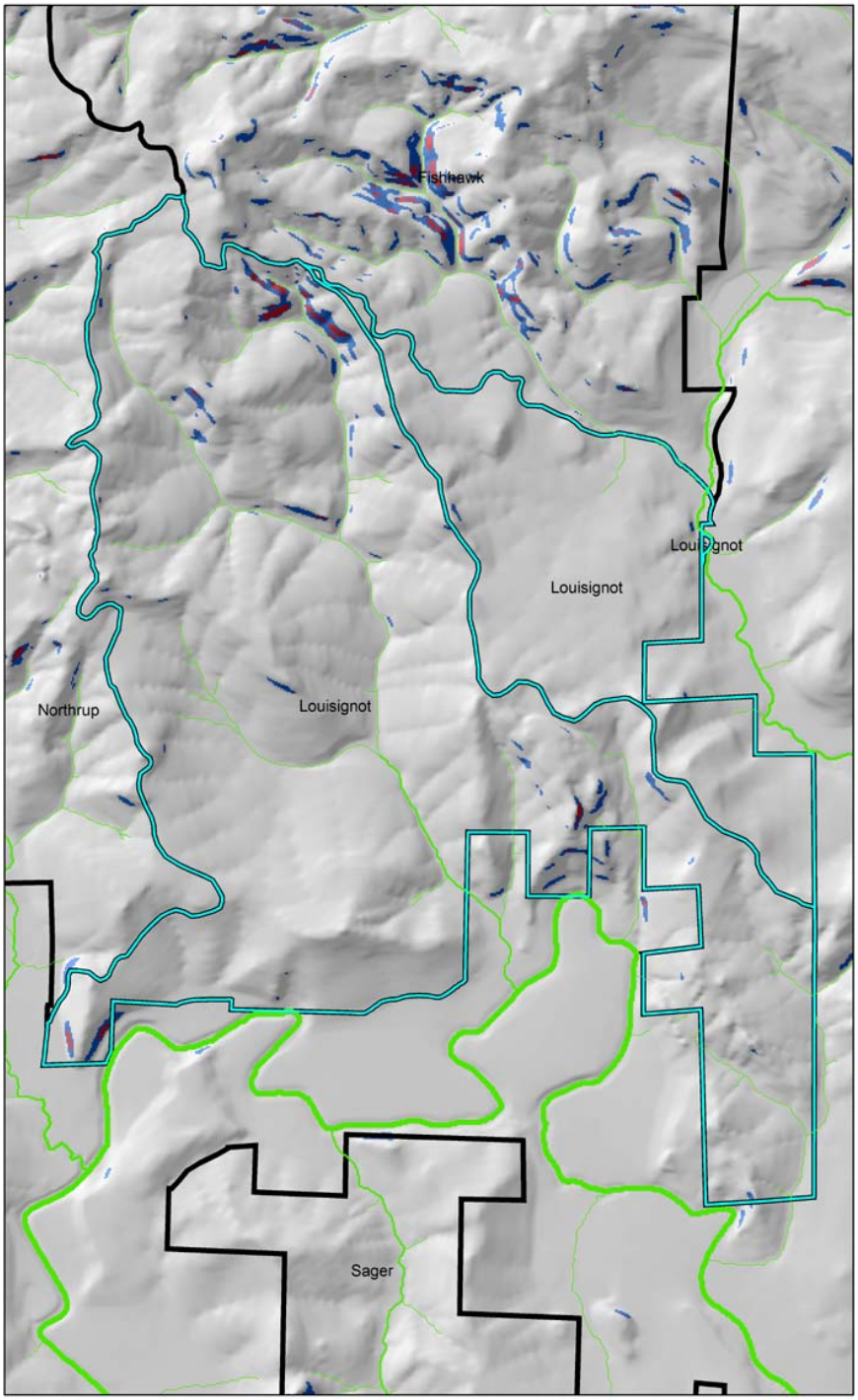

Figure D-20. Slope gradient map for the Louisignot Management Basin. Refer to the Legend in Figure D-7.

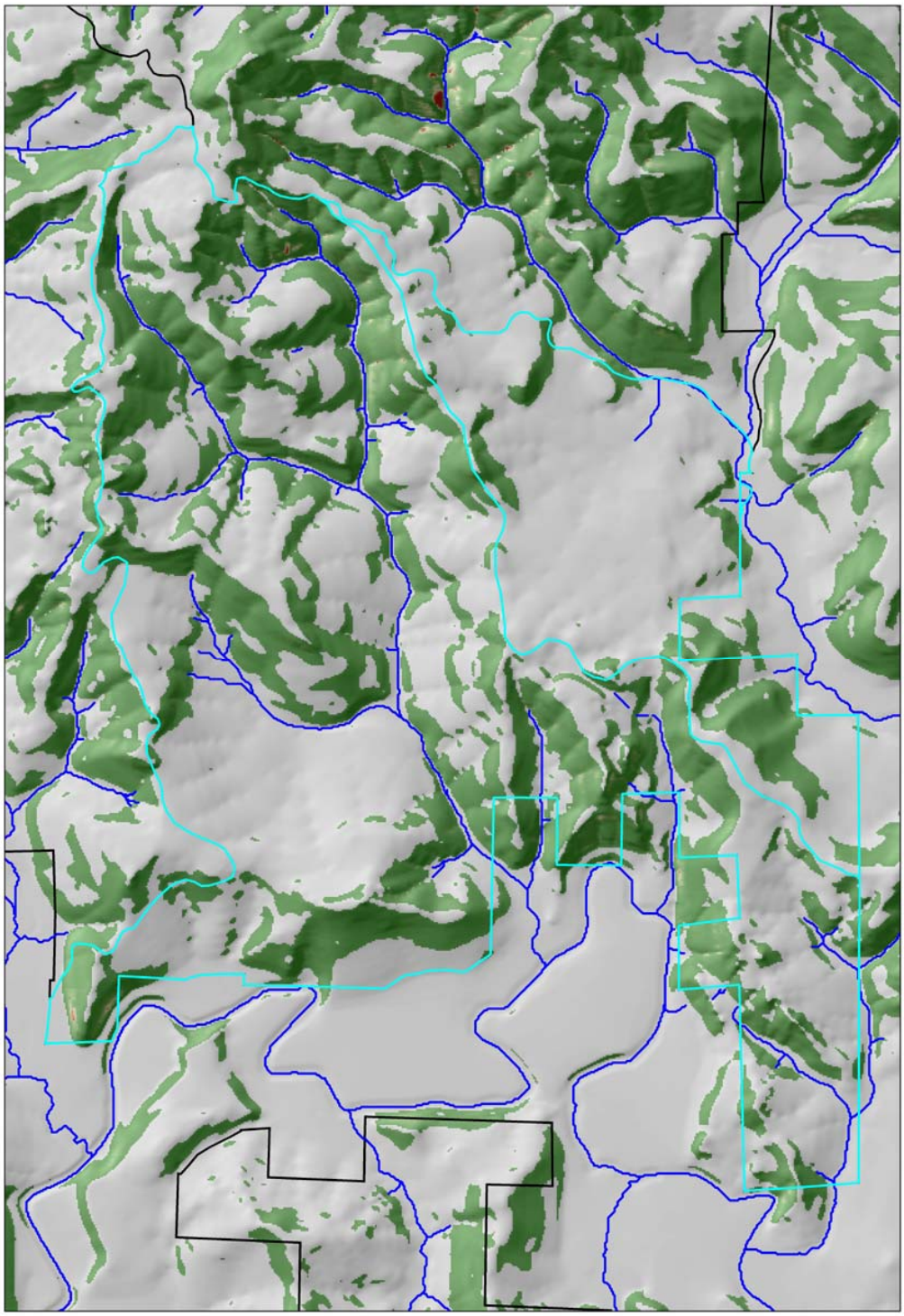

Figure D-21. Predicted landslide density for the Louisignot Management Basin. Refer to the Legend in Figure D-7; the gray areas have no predicted landslide density.

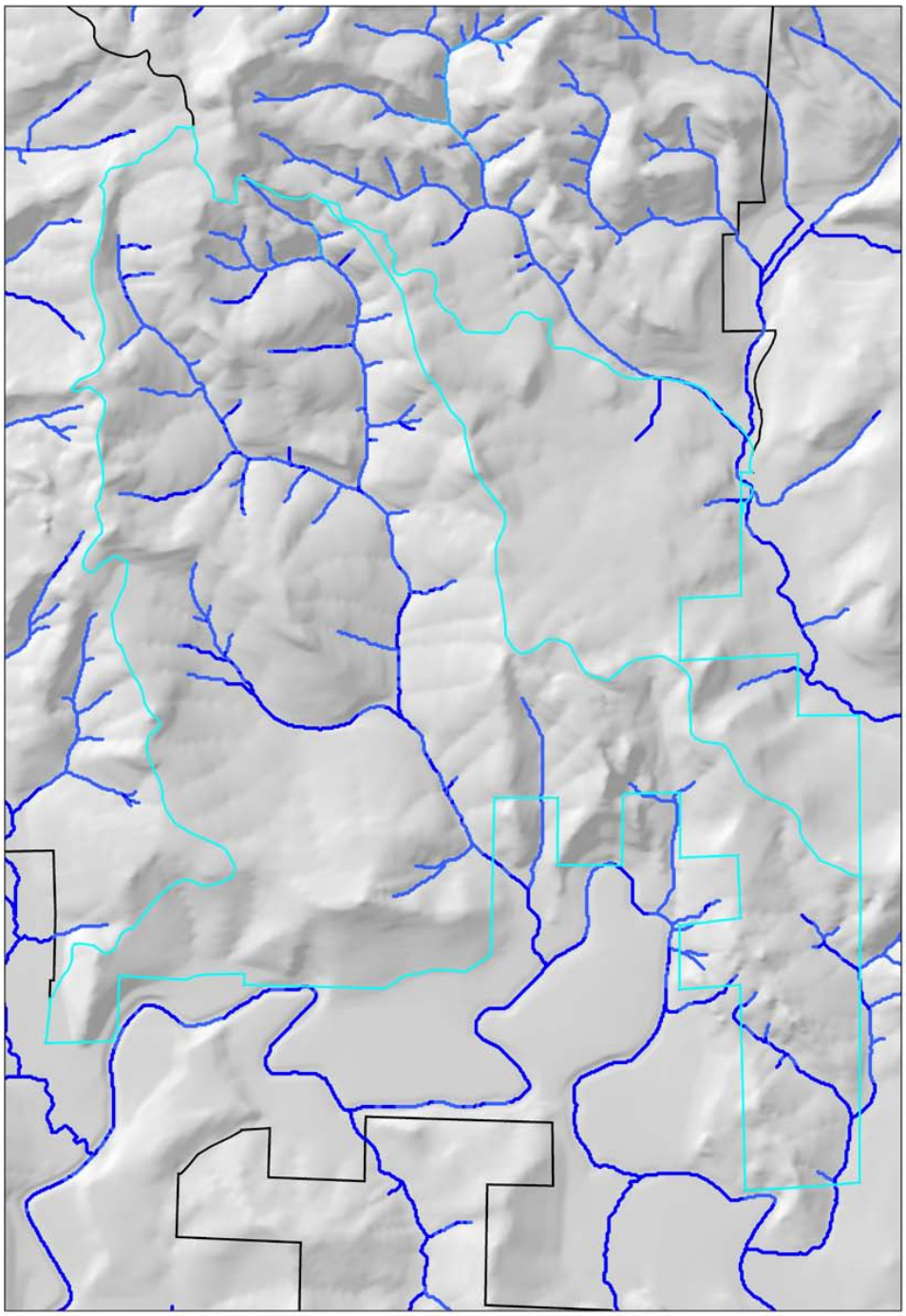

Figure D-22. Predicted debris flow probability for the Louisignot Management Basin. Refer to the Legend in Figure D-7. The predicted probabilities reflect cumulative landslide densities (that could trigger debris flows) and not individual pixel-based landslide potential shown in the landslide density map.

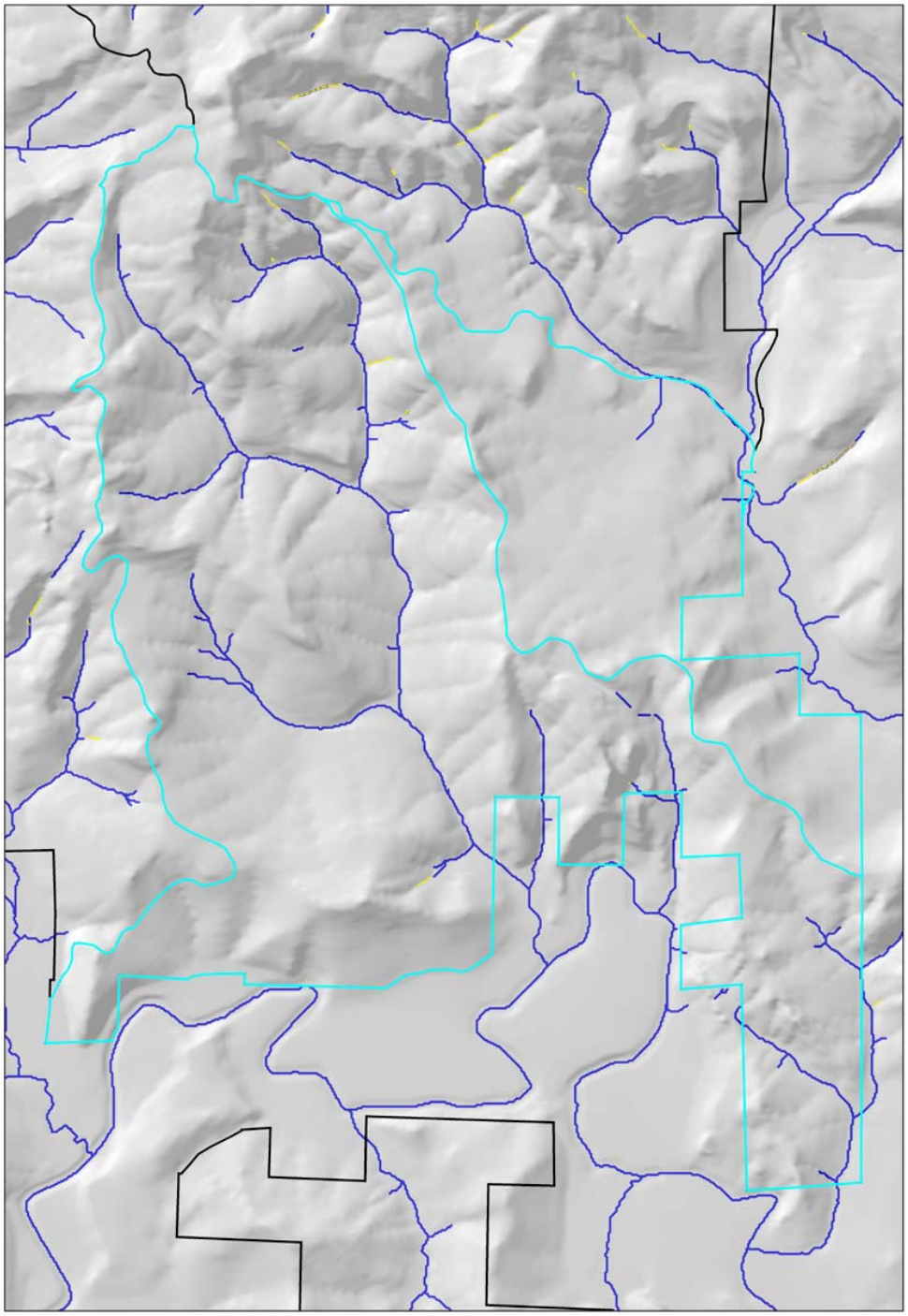

Figure D-23. Predicted headwater streams that contributed wood to fish-bearing channels by debris flows for the Louisignot Management Basin. Refer to the Legend in Figure D-7; predictions apply to headwater streams only. The predicted probabilities reflect cumulative landslide densities (that could trigger debris flows) and not individual pixel-based landslide potential shown in the landslide density map.

HAMILTON MANAGEMENT BASIN

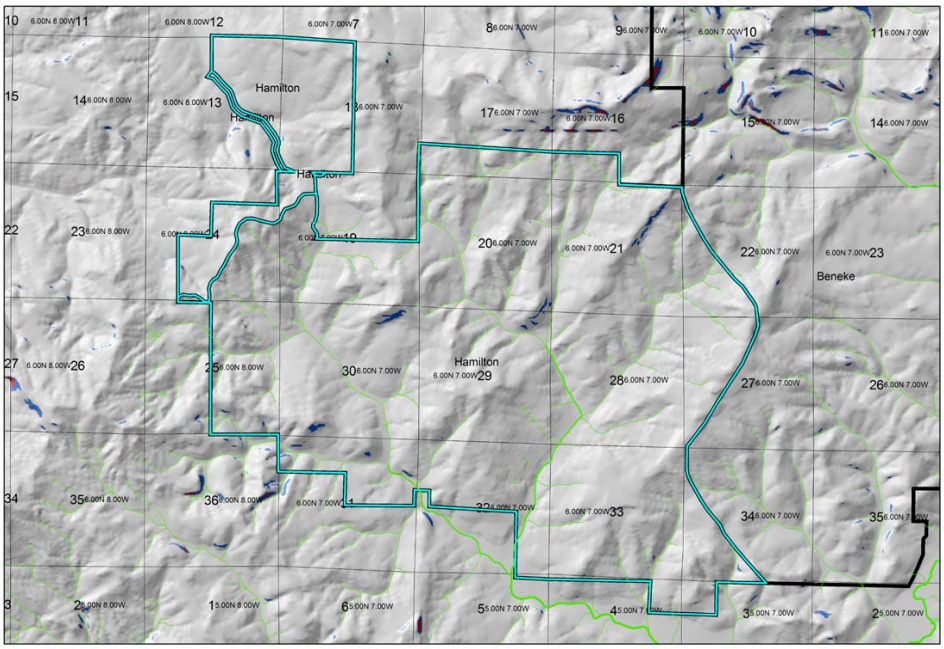

Figure D-24. Slope gradient map for the Hamilton Management Basin. Refer to the Legend in Figure D-7.

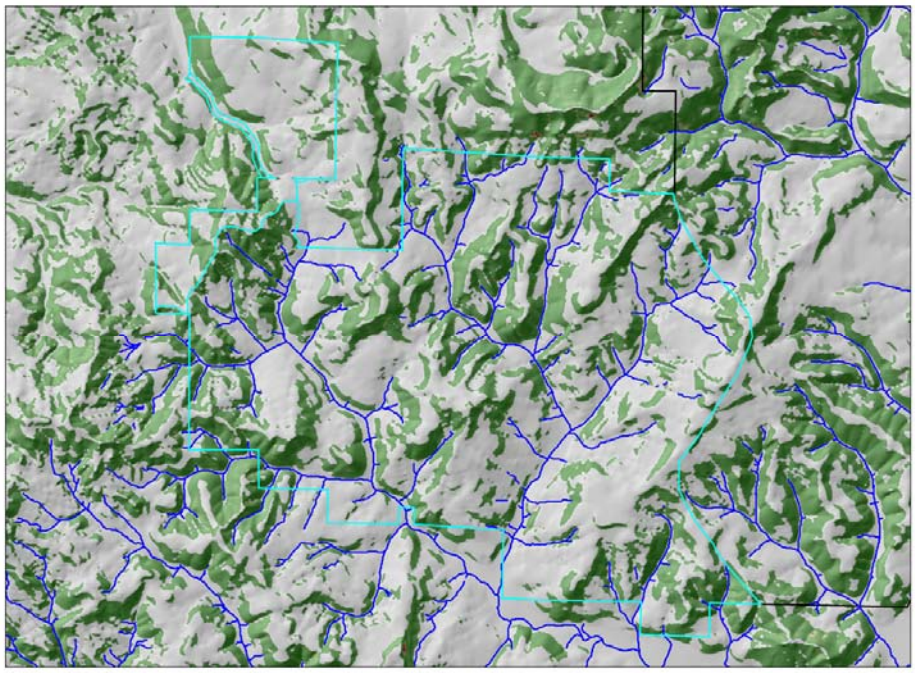

Figure D-25. Predicted landslide density for the Hamilton Management Basin. Refer to the Legend in Figure D-7; the gray areas have no predicted landslide density.